The Through-Thickness Compressive Strength of a Composite Sandwich Panel With a Hierarchical Square Honeycomb Sandwich Core

F. Côté

B. P. Russell

V. S. Deshpande

N. A. Fleck

Department of Engineering,
University of Cambridge,
Cambridge CB2 1PZ, UK

Sandwich panels with aluminum alloy face sheets and a hierarchical composite square honeycomb core have been manufactured and tested in out-of-plane compression. The prismatic direction of the square honeycomb is aligned with the normal of the overall sandwich panel. The cell walls of the honeycomb comprise sandwich plates made from glass fiber/epoxy composite faces and a polymethacrylimide foam core. Analytical models are presented for the compressive strength based on three possible collapse mechanisms: elastic buckling of the sandwich walls of the honeycomb, elastic wrinkling, and plastic microbuckling of the faces of the honeycomb. Finite element calculations confirm the validity of the analytical expressions for the perfect structure, but in order for the finite element simulations to achieve close agreement with the measured strengths it is necessary to include geometric imperfections in the simulations. Comparison of the compressive strength of the hierarchical honeycombs with that of monolithic composite cores shows a substantial increase in performance by using the hierarchical topology.
[DOI: 10.1115/1.3086436]

Keywords: honeycombs, composite, strength, sandwich panels

1 Introduction

[1]The concept of a thick and light core sandwiched between two strong thin facings has been used to produce stiff and lightweight panels since the 19th century [1]. The underlying theory and design methods for sandwich constructions are well known [2,3]. For example, it is generally recognized that the stiffness and strength of a sandwich panel under macroscopic loading (bending, end loading, and torsion) are sensitive to the thickness of the core and to the in-plane properties of the face sheets.

Stochastic foam and periodic lattice materials are two broad classes of core increasingly employed in sandwich construction [4]. Closed cell foams behave as a continuous core and provide a continuous interface for bonding to the faces, but they possess a low specific stiffness and strength. In contrast, lattice materials have a high specific stiffness and strength due to their high nodal connectivity [5]. Three categories of periodic lattice materials have been developed: (i) prismatic cores, (ii) 3D trusses, and (iii) honeycombs. In this study we shall explore the properties of a *hierarchical sandwich core* in the form of a square honeycomb.

Hexagonal honeycombs made from Nomex or from aluminum alloy are extensively employed in sandwich construction due to their high specific stiffness and strength in out-of-plane compression and in longitudinal shear. However, these hexagonal honeycombs have low values of in-plane stiffness and strength due to a nodal connectivity of only 3 [6]. Square honeycombs have a higher nodal connectivity of 4, and thereby have enhanced in-plane properties. Further, the out-of-plane properties of the square honeycomb are comparable to those of the hexagonal honeycombs, see, for example, recent measurements of out-of-plane compressive strength [7] and of longitudinal shear strength [8].

It is of interest to explore sandwich panel cores that possess a high stiffness and strength yet have a low density. Honeycomb cores made from monolithic composite sheets have a higher specific stiffness and strength than many metallic honeycombs. The out-of-plane compressive strength of sandwich panels with a composite or metallic honeycomb core is limited by the elastic buckling of the cell walls when the core has a low relative density ($\bar{\rho} < 0.05$). Here, we shall explore a strategy for increasing the elastic buckling strength of the cell walls by employing sandwich construction for the cell walls [9]. The microstructure is *hierarchical* in topology: The *macroscopic* sandwich panel comprises aluminum alloy face sheets and a square honeycomb core, with the cell walls of the core made from *mesoscopic* sandwich panels (see Fig. 1(*a*)). These mesoscopic panels comprise a polymethacrylimide (PMI) foam sandwiched between woven glass fiber/epoxy composite faces.

The outline of this paper is as follows. First, competing collapse mechanisms are considered for the out-of-plane compressive strength of a sandwich panel with a square honeycomb core. Analytical expressions are taken from the literature for each mechanism, and the dominant collapse mechanism is plotted on a map with geometry as axes. Second, an experimental investigation is conducted to probe the accuracy of the analytical predictions. Third, the measurements and analytical predictions are compared with three-dimensional (3D) finite element (FE) simulations, and the role of geometric imperfection in dictating compressive strength is assessed. Finally, the measured and predicted compressive strengths are compared with that of monolithic composite square honeycombs.

[1]Trade name of Dupont referring to an aramid paper impregnated with epoxy resin.

Contributed by the Applied Mechanics Division of ASME for publication in the JOURNAL OF APPLIED MECHANICS. Manuscript received August 9, 2007; final manuscript received January 11, 2009; published online July 23, 2009. Review conducted by Kenneth M. Liechti.

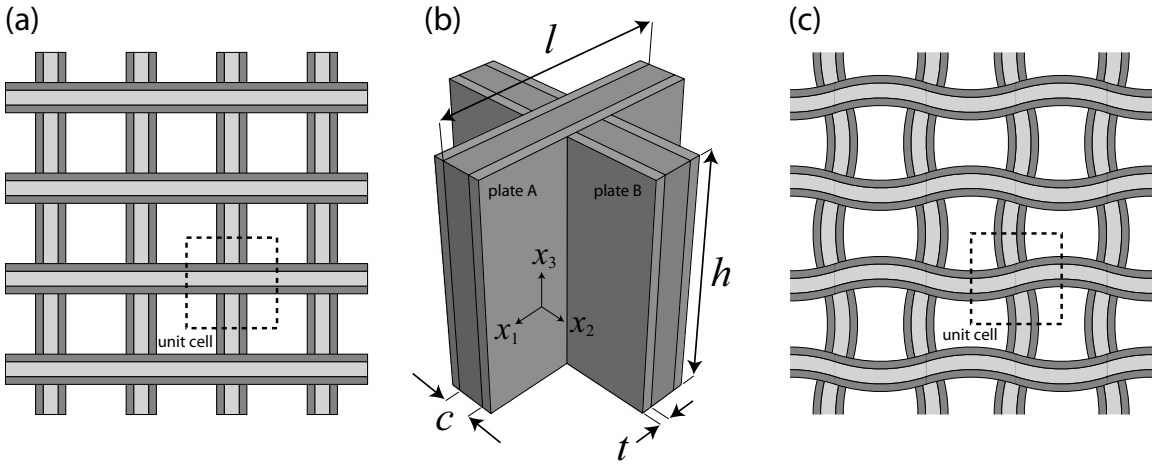

Fig. 1 (*a*) Sketch of a square honeycomb core with the cell walls of the core made from a mesoscopic sandwich panels, (*b*) schematic of the unit cell and geometrical parameters employed in the analytical model and finite element analysis, and (*c*) torsional-axial buckling mode of square honeycomb core

2 Analytical Models for the Competing Collapse Modes

2.1 Geometry of Core and the Imposed Loading. Consider a square honeycomb core perfectly bonded to rigid face sheets. The core has sandwich walls with square cells of side-length l and height h, and the prismatic direction of the honeycomb core is aligned with the out-of-plane direction of the overall honeycomb (Fig. 1(*b*)). The sandwich walls comprise an isotropic foam of thickness c and density ρ_c bonded between two orthotropic elastic faces, each of thickness t and density ρ_f. This representation is appropriate for the material system studied herein: woven glass fiber/epoxy faces and a PMI foam core.

The macroscopic sandwich panel is subjected to an out-of-plane compressive stress σ; consequently, each cell wall is subjected to a line load P per unit length where

$$P = \sigma \frac{l}{2} \tag{1}$$

while the effective density ρ of the square honeycomb core is

$$\rho = 2\frac{t}{l}\left(2 - \frac{(2t+c)}{l}\right)\rho_f + \frac{c}{l}\left(2 - \frac{(2t+c)}{l}\right)\rho_c \tag{2}$$

Three collapse mechanisms are considered: (i) elastic buckling of the square honeycomb, (ii) elastic face wrinkling of the mesoscopic sandwich panels that make up the cell walls of the square honeycomb, and (iii) plastic microbuckling of the composite face sheets of the mesoscopic sandwich panels. The out-of-plane compressive strength of the macroscopic sandwich panel is dictated by the collapse mechanism that has the lowest value of line load P_{cr} for any given set of geometric and material parameters. The compressive strengths for mechanisms (i) and (ii) above are sensitive to the elastic moduli of the foam core in the mesoscopic sandwich panels. We proceed by summarizing the elastic moduli for a closed-cell foam.

2.2 Elastic Properties of Closed-Cell Foams. Gibson and Ashby [4] extensively reviewed the mechanical properties of open- and closed-cell foams. They showed that Young's modulus E_c and the shear modulus G_c of an isotropic, closed-cell foam are directly related to the relative density $\bar{\rho} \equiv \rho_c/\rho_s$, where ρ_s is the density of the parent, solid polymer, such that

$$\frac{E_c}{E_s} \approx \phi^2\left(\frac{\rho_c}{\rho_s}\right)^2 + (1-\phi)\left(\frac{\rho_c}{\rho_s}\right) \tag{3}$$

and

$$G_c \approx \tfrac{3}{8}E_c \tag{4}$$

Here, E_s is Young's modulus of the solid polymer and ϕ is the volume fraction of cell wall material contained within the cell edges. For the PMI foam investigated in Sec. 3 of the present study, we assume that $E_s = 3600$ MPa, $\rho_s = 1250$ kg m^{-3}, and $\phi = 0.6$ [4].

2.3 Elastic Buckling of the Square Honeycomb Core. A recent experimental study [7] on the compressive collapse of square honeycombs made from type 304 stainless steel suggests that the elastic buckling mode resembles torsional-axial buckling of a square tube (i.e., local buckling of the walls) with built-in top and bottom edges, as sketched in Fig. 1(*c*). Finite element simulations reported later in the current study confirm this mode of elastic buckling for the sandwich-walled square honeycomb. This buckling mode is modeled by the buckling of a single plate with fully clamped top and bottom edges and simply supported sides. Ericksen and March [10] analyzed this reduced problem for a sandwich plate made from orthotropic faces and an orthotropic core, and we make direct use of their analytical results. The bifurcation line load reads

$$P_{\text{buck}} = \frac{K\pi^2 D}{l^2} \tag{5}$$

where K is a buckling coefficient as prescribed by Ericksen and March [10] and D is the bending stiffness of the sandwich plate. In our problem, we consider a sandwich plate made from orthotropic composite faces of identical thickness t. Upon neglecting the contribution from the foam core to the overall bending stiffness D we have

$$D = \frac{\sqrt{E_{1f}E_{3f}}}{1 - \nu_{13f}\nu_{31f}}\frac{t(c+t)^2}{2} \tag{6}$$

where E_{if} and ν_{ijf} are Young's modulus and Poisson's ratios of the orthotropic faces along the $x_i = (x_1, x_3)$ directions, as defined in Fig. 1(*b*). (For the composite faces considered below Young's moduli are equal along directions x_1 and x_3.)

The formula for the buckling coefficient K is explicit but lengthy and is omitted here. They are functions of geometry (c, t, l, and h as defined in Fig. 1(*b*)), of the enforced boundary conditions along the edges of the plate, of Young's modulus E_c and shear modulus G_c for the isotropic core, as well as of the shear modulus, Young's moduli, and Poisson ratios of the faces in the $x_1 - x_3$ plane.

Table 1 Measured properties of the woven glass fiber/epoxy faces and a PMI foam core

Material	Density (kg m^{-3})	Compressive strength (MPa)	Young's modulus (GPa)	Shear modulus (GPa)	Poisson's ratio (−)
GFRP	ρ_f=1957	σ_f=525	E_{3f}=32	G_{31f}=4	ν_{31f}=0.15
PMI foam	ρ_c=75	1.45	E_c=0.089	G_c=0.038	ν_c=0.16

2.4 Elastic Face Wrinkling. The sandwich plates in the walls of the square honeycomb can collapse by an alternative mechanism to those considered by Ericksen and March [10]: elastic wrinkling of the faces of the sandwich plate. This wrinkling mode is a local instability associated with short wave buckling of the faces of the mesoscopic sandwich plate and occurs when a compressive stress within the faces attains a critical value, see, for example, Ref. [3]. Assume that the sandwich plate is loaded along the x_3-direction. Then, the critical line load P_{wrink} in the sandwich plate depends on Young's modulus E_{3f} in the face and on the moduli (E_c, G_c) of the core such that

$$P_{\text{wrink}} = 1.7t(E_{3f}E_cG_c)^{1/3} \tag{7}$$

This formula gives the bifurcation stress for the perfect structure in the absence of geometric imperfection. It is appreciated that the presence of imperfections knocks down this strength by a factor of about 2 for most practical sandwich structures [3].

2.5 Plastic Face Microbuckling. It is generally recognized that the composite faces of a sandwich plate can fail by plastic microbuckling, particularly when the composite has wavy fibers due to its woven construction, see Ref. [11] for details on plastic microbuckling. Here, we treat the microbuckling strength σ_f as an intrinsic material property. Consequently, the microbuckling line load in the x_3-direction on the sandwich plates of the square honeycomb reads

$$P_{\text{mb}} = 2t\sigma_f \tag{8}$$

where we neglect any contribution from the compression of the core.

2.6 Collapse Mechanism Map. In the remainder of this study we shall limit our attention to the practical case of square honeycombs with aspect ratio $h/l=1$, thereby reducing the number of independent geometric variables. The regimes of dominance of the collapse modes can then be illustrated in a collapse mechanism map, with axes t/c and l/c. In construction of the map, it is assumed that the operative collapse mode is the one associated with the lowest line load for any given geometry.

A collapse mechanism map has been constructed for the materials used in the experimental study, as listed in Table 1. This map is plotted in Fig. 2(*a*); it assumes a foam core of relative density $\bar{\rho}$=6% as used in the experiments. In addition, a map is shown in Fig. 2(*b*) for a higher relative density of foam core $\bar{\rho}$=20% for comparison purposes. Although such high density PMI foams exist, they are more expensive and less available than the $\bar{\rho}$=6% and so no experiments were conducted on the higher density foam. Contours of nondimensional compressive strength $\bar{\sigma} \equiv P_{\text{cr}}/P_{\text{mb}}$ have been added to the maps, upon treating the microbuckling line load as an intrinsic reference property of the sandwich plates, independent of (c, l, h).

The collapse mechanism map of Fig. 2(*a*) ($\bar{\rho}$=6%) displays two failure modes: Core buckling dominates the map with a much smaller regime of face wrinkling. The dominance of core buckling can be traced to the fact that this mechanism is sensitive to a low value of shear modulus in the foam core. Now increase $\bar{\rho}$ to 20%. The buckling load and face wrinkling loads increase, and microbuckling replaces face wrinkling as an active mechanism, see Fig. 2(*b*).

The accuracy of the failure map given in Fig. 2(*a*) has been partially assessed by conducting a series of experiments on the geometries shown in the map. It was not practical to cover a much larger regime of the map due to manufacturing and testing constraints. These experiments are now reported.

3 Experimental Investigation

A series of compressive tests was performed on square honeycombs with cell walls made from glass fiber/epoxy composite face sheets and a $\bar{\rho}$=6% foam core.

3.1 Manufacturing Technique. The sandwich cores were made from a closed-cell PMI foam of relative density $\bar{\rho} \approx 6\%$ (trade name Rohacell 71 IG) and thickness c=5.7 mm. This foam

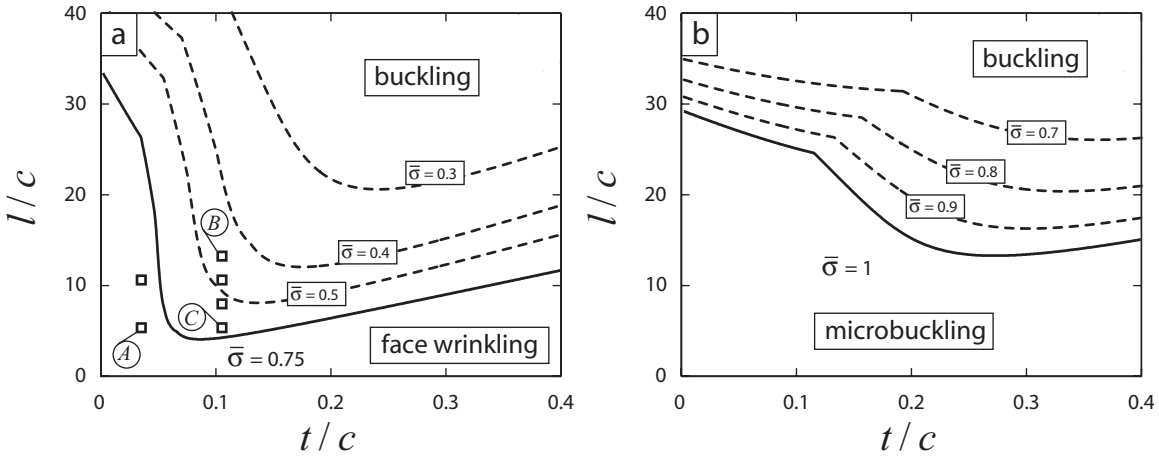

Fig. 2 Collapse mechanism map and contours of normalized strength $\bar{\sigma} \equiv P_{\text{cr}}/P_{\text{mb}}$ of the hierarchical square honeycomb made from elastic face and polymeric foam core of relative density (*a*) $\bar{\rho}$=0.06 and (*b*) $\bar{\rho}$=0.20. The six tested geometries are marked on the map (*a*).

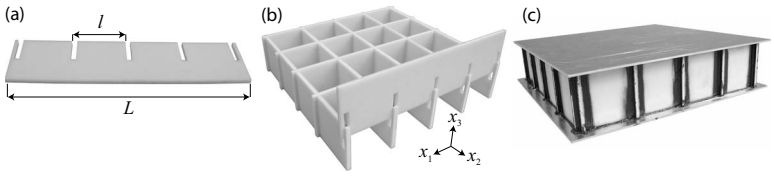

Fig. 3 Photographs a specimen with l=75 mm and t=0.6 mm demonstrating the manufacturing technique: (*a*) a waterjet machined panel, (*b*) the assembling technique, and (*c*) the final product

was selected for its low density (ρ_c=75 kg m^{-3}) and its capacity to sustain a pressure up to 0.35 MPa at 125°C, allowing autoclave curing.

The faces were made from one to three stacked plies of eight harness satin weave 7781 E-glass pre-impregnated (42 wt % of resin before curing) in a toughened epoxy matrix resin (trade name ACG MTM28/GF0100). This prepreg was selected for its low curing temperature of 120°C, high damage tolerance, and ability to bond directly to the PMI foam without additional adhesive. After curing, each ply has a thickness of 0.2 mm, a volume fraction of 55% glass fibers, and a density of ρ_f=1957 kg m^{-3}. The manufacturing sequence of the macroscopic square honeycomb is as follows.

(i) The PMI foam was dried for 2 h in a furnace at 100°C in order to reduce the moisture content. Layers of prepreg were placed symmetrically on each side of the foam, and the 0–9 deg orientations of the laminate were aligned with the x_1 and x_3 directions (see Fig. 1). Air pockets between each composite layer were removed by debulking the panel at room temperature under vacuum for 3 min.

(ii) The sandwich panel was then cured in an autoclave for 1 h at 120°C and a gauge pressure of 0.25 MPa, with the usual vacuum bagging technique.

(iii) The sandwich panel was cropped by a waterjet cutting machine into long strips of height $h=l$ and length $L=4l+2\Delta L$, where ΔL is a small overhang length set at 5 mm, see Fig. 3(*a*). Cross-slots were waterjet cut into the strips. These slots were of spacing l and of width $(c+2t+e)$, where e is a clearance of 0.1 mm to provide a sufficiently tight fit during honeycomb assembly.

(iv) Structural adhesive (trade name 3M Scotch-Weld DP490) was applied over the slot areas, and the honeycomb was assembled by slotting together the strips (Fig. 3(*b*)). Finally, the honeycomb was bonded to two 2014-T3 aluminum alloy face sheets of thickness 3 mm using the same structural adhesive as for the core (Fig. 3(*c*)).

A series of compression tests was performed on the macroscopic sandwich panels. Each specimen comprised 4×4 cells with a cell size l varying from 30 mm to 75 mm and a face thickness t between 0.2 mm and 0.6 mm. Consequently, the core density ρ varied from 38 kg m^{-3} to 167 kg m^{-3}. The cell sizes and densities of the tested specimens are listed in Table 2.

3.2 Material Properties of the Composite-Foam Sandwich Plates of the Square Honeycomb. The in-plane microbuckling strength σ_f, Young's modulus $E_{1f}=E_{3f}$, and Poisson ratio ν_{13} of

Table 2 Geometry, predicted compressive strength, and measured compressive strength of the macroscopic sandwich panels with a square honeycomb core

t (mm)	l (mm)	ρ (kg m^{-3})	Predicted strength (MPa)				Measured strength (MPa)
			Wrinkling	Microbuckling	Buckling	First eigenvalue	
0.2	60	38	5.4	7.2	8.0	5.2	3.1
0.2	30	73	10.8	14.4	17.1	9.8	4.3
0.6	75	71	13.0	17.3	8.4	8.4	7.8
0.6	60	75	16.3	21.7	11.1	11.2	10.9
0.6	45	116	21.7	28.9	16.3	16.4	11.7
0.6	30	167	32.5	43.3	29.1	32.4	15.8

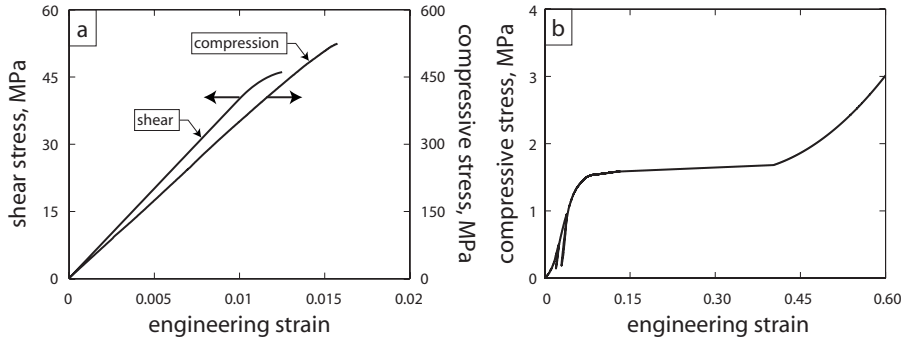

Fig. 4 (*a*) The measured compressive and shear responses of the eight harness satin weave 7781 E-glass/epoxy composite and (*b*) the measured uniaxial compressive response of the PMI foam (Rohacell 71 IG) used for the mesoscopic sandwich panel

the composite face sheet were measured by compressing the 0–90 deg composite along the x_3-direction within a Celanese test rig [12] at a nominal strain rate of 10^{-4} s^{-1}. The Celanese tests were performed on specimens of width 10 mm, thickness 2 mm, and gauge length 8 mm. Strain gauge rosettes were adhered to both faces of the specimen and confirmed that the degree of macroscopic bending in the tests was negligible. The measured compressive stress versus strain response is shown in Fig. 4(*a*); the measured axial Young's modulus is $E_{3f}=32$ GPa, the Poisson's ratio is $\nu_{31f}=0.15$, and the microbuckling strength is $\sigma_f=525$ MPa. These values are of the order expected from the specification given by the manufacturer.

The shear elastic properties of the composite faces were measured via a uniaxial tensile test on ± 45 deg material [13]. We denote the applied tensile stress as σ_x, and the corresponding axial strain and transverse strain as ε_x and ε_y, respectively. Then, the shear stress τ versus shear strain γ relation is obtained via the connections $\tau=\sigma_x/2$ and $\gamma=\varepsilon_x-\varepsilon_y$. The shear modulus G_{31f} follows immediately as the initial slope of the τ versus γ response. These uniaxial tensile tests were conducted on specimens of width 20 mm, thickness 0.4 mm, and gauge length 50 mm at a nominal strain rate of 10^{-4} s^{-1}. Strain gauge rosettes were used on both sides of the coupons, and the measured shear modulus was $G_{31f}=4.0$ GPa. The derived shear stress and strain response is included in Fig. 4(*a*).

The uniaxial compressive response of the Rohacell 71 IG foam core was measured by compressing cylindrical specimens of diameter 50 mm and height 6 mm between lubricated flat platens at an applied nominal strain rate of 10^{-3} s^{-1}. The nominal stress was estimated from the load cell of the test machine while the applied strain was deduced from the relative displacement of the top and bottom platens using a laser extensometer. The measured response is plotted in Fig. 4(*b*) and displays an initial elastic response and plateau strength of approximately 1.5 MPa and densification of the foam commences at a nominal compressive strain of 0.45. The elastic modulus of the foam was determined by conducting an unloading/reloading cycle, as shown in Fig. 4(*b*). However, difficulties in adhering strain gauges to the foam specimens mean that elastic Poisson's ratio was unable to be extracted from these compression tests.

We measured the elastic properties of the Rohacell 71 IG foam core using a vibro-acoustic technique based on Chaldni's law [14]. For an isotropic material, the method consists of identifying the x-mode resonance frequency f_x and ring mode resonance frequency f_o of square plates with free edges. This technique is simple and requires basic equipment, as discussed in Ref. [14]. The square plate is simply supported by soft blocks of foam and excited by a loudspeaker mounted beneath it. The loudspeaker is driven by a sinusoidal wave generator, and the frequency is adjusted to resonance. Chaldni's patterns are revealed by sprinkling a light powder on the surface. Once the f_x and f_o frequencies have been measured, both Young's modulus E_c and Poisson's ratio ν_c are determined via the prescriptions

$$\nu_c \approx 1.48\left[\frac{f_o^2-f_x^2}{f_o^2+f_x^2}\right] \tag{9}$$

$$E_c \approx 0.46(1-\nu_c^2)(f_o^2+f_x^2)\rho_c a^4/c^2 \tag{10}$$

where a is the square plate length, ρ_c is the plate density, and c is the plate thickness.

In these measurements, a Rohacell 71 IG foam square plate of dimension $a=315$ mm, $\rho_c=75$ kg m^{-3}, and $c=5.7$ mm was employed. The resonance frequencies f_x and f_o were found to be 61.9 Hz and 68.6 Hz, respectively, leading to $\nu_c=0.16$ and $E_c=89$ MPa. These values are within a few percent given by Eq. (3) and the textbook values $E_s=3600$ MPa, $\rho_s=1250$ kg m^{-3}, and $\phi=0.6$ [4].

3.3 Measured Compressive Response of the Macroscopic Sandwich Panel With Square Honeycomb Core. Compression tests were performed on the macroscopic sandwich panels using a 1000 kN servohydraulic frame test machine and an applied macroscopic nominal strain rate of 10^{-4} s^{-1}. The macroscopic compressive stress σ on the core was inferred from the load cell of the test machine while the average through-thickness compressive strain ε was deduced from the relative displacement of the top and bottom faces of the sandwich panel, upon making used of two laser extensometers.

The measured out-of-plane compressive response of each sandwich panel is plotted in Fig. 5. All display an initial elastic response, with a peak load at a strain level $\varepsilon<0.02$ followed by a catastrophic drop in load. Each test was terminated after the drop in load, and the specimens were then visually examined to determine the collapse mechanism. It was not possible to use visual evidence to distinguish between the three anticipated collapse modes of elastic buckling, face wrinkling, and plastic microbuckling: In all cases the composite faces of the square honeycomb creased in bending, with no evidence of the initial cause of the failure.

The analytical predictions of compressive strength (Eqs. (1), (5), (7), and (8)) for the three competing collapse modes have been added to Fig. 5. In most cases all three analytical predictions are substantially higher than the measured strength. The tests reported in Figs. 5(*c*) and 5(*d*) are the exceptions to this observation: In these cases the elastic buckling strength is comparable to the measured strength. Note that these two geometries lie remote from the elastic buckling/face wrinkling boundary, as plotted in Fig. 2(*a*). In order to improve the accuracy of prediction, finite element simulations are performed, and the imperfection sensitivity is assessed.

4 Finite Element Modeling

4.1 Model Details. Finite element calculations of the through-thickness compressive response of the sandwich panels with a square honeycomb core were performed using the finite element package ABAQUS standard (Hibbitt, Karlsson & Sorensen, Inc. (HKS)). All simulations reported here are performed on the unit cell shown in Fig. 1(*b*) in the form of a cruciform section, including the nonlinear effects of large displacements.

The unit cell of the square honeycomb was modeled using linear 3D brick elements, i.e., C3D8R following ABAQUS notation. Typically, the model comprised four brick elements through the thickness of each composite face sheet and five to ten brick elements through the depth of the foam core. In order to avoid excessive distortion, the element aspect ratio was kept below 5 for all simulations. One exception is that the specimen with $t=0.2$ mm and $l=60$ mm was modeled with an aspect ratio of 10 in order to reduce the model size. This meshing rule assures convergence but leads to large models, for example, the model with $t=0.6$ mm and $l=75$ mm contains over 10^6 degrees of freedom.

In order to capture the torsional-axial buckling mode (Fig. 1(*c*)) and the face wrinkling mode, antiperiodic boundary conditions were imposed on the outer plate edges of the cruciform section. All nodes on the top and bottom of the unit cell were fully clamped. Loading was specified by prescribing an increasing relative vertical displacement δ between the top and bottom faces.

The PMI foam was modeled as an isotropic elastic-ideally plastic solid, using the properties values presented in Sec. 3. The post-yield behavior was modeled with the crushable foam formulation available in ABAQUS using an associated flow rule. The ratio of the uniaxial compressive strength to the hydrostatic strength was set to $\sqrt{3}$, and the tensile and compressive hydrostatic strengths were assumed to be equal. With these assumptions the crushable foam model in ABAQUS reduces to the Deshpande and Fleck [15] foam model with plastic Poisson's ratio of 0. Mild

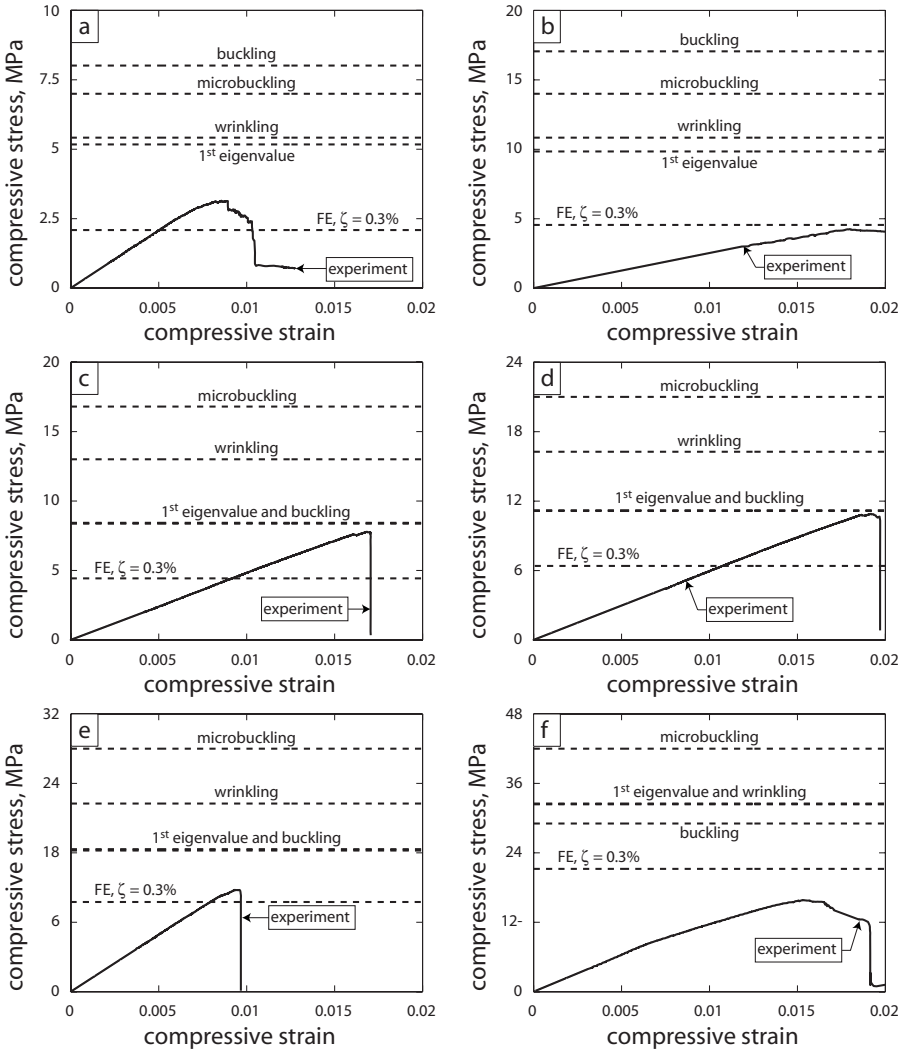

Fig. 5 The measured compressive response of square honeycomb specimens with (*a*) $l=60$ mm and $t=0.2$ mm, (*b*) $l=30$ mm and $t=0.2$ mm, (*c*) $l=75$ mm and $t=0.6$ mm, (*d*) $l=60$ mm and $t=0.6$ mm, (*e*) $l=45$ mm and $t=0.6$ mm, and (*f*) $l=30$ mm and $t=0.6$ mm. Also added in the figure is the compressive strength predicted by analytical models, FE buckling analysis, and FE static analysis with an imperfection of $\varsigma \equiv w/l=0.3\%$.

volumetric hardening of the plastic response of the foam was included in order to assure numerical stability.

The woven glass fiber/epoxy composite was treated as an orthotropic solid with the in-plane measured properties stated in Sec. 3. Consider the representative sandwich plate A, as shown in Fig. 1(*b*). The properties in the direction normal to that of the composite plates were taken as $E_2=7.5$ GPa, $G_{12}=G_{32}=4.0$ GPa, and $\nu_{12}=\nu_{32}=0.15$. In order to mimic plastic microbuckling, it was assumed that the composite was modeled as an elastic-ideally plastic solid. J2 flow-theory was adopted with a yield strength equals to the microbuckling strength ($\sigma_f=525$ MPa) and a mild isotropic hardening to assure numerical stability. Although this description is only approximate it suffices to capture the onset of microbuckling for the in-plane uniaxial stress state imposed on the composite layers.

4.2 Elastic Buckling Analysis. The FE method has been used to determine the lowest buckling load (the first eigenvalue). The compressive strength is compared with the analytical models and the measured response in Fig. 5 and in Table 2. In general, the predicted first eigenvalues are in good agreement with the lowest collapse load predicted analytically by the three competing mechanisms. There is one exception: The analytical model underestimates the compressive strength of the specimen with $t=0.6$ mm and $l=30$ mm. It is argued that this is due to the fact that the analytical buckling model is inaccurate for stubby plates, $l/c<6$. The predicted eigenmode resembles the assumed buckling mode of elastic bucking model and resembles the face wrinkling mode, depending on the geometry considered. Consider, for example, the geometry as specified by $t/c=0.035$ and $l/c=5.25$ and label this specimen A in Fig. 2(*a*). This specimen undergoes elastic face wrinkling according to both the analytical model and the FE simulation, see Fig. 6(*a*) for the observed eigenmode. Second, consider specimens with $t/c=0.105$, and $l/c=10.5$ and $l/c=5.25$, and label them B and C in Fig. 2(*a*). The lowest FE eigenmode for these two specimens is given in Figs. 6(*b*) and 6(*c*), respectively. Plainly the modes are elastic buckling of the sandwich plates, and these modes are in agreement with the modes predicted by the analytical model of Ericksen and March [10].

4.3 Imperfection Sensitivity. The discrepancy between measured compressive strength and the extracted eigenvalues indicates a possible sensitivity to geometric imperfection. This sensitivity was scoped by FE calculations of the collapse response for sandwich plates with initial imperfections in the shape of the first elastic eigenmode. The magnitude of the initial imperfection is

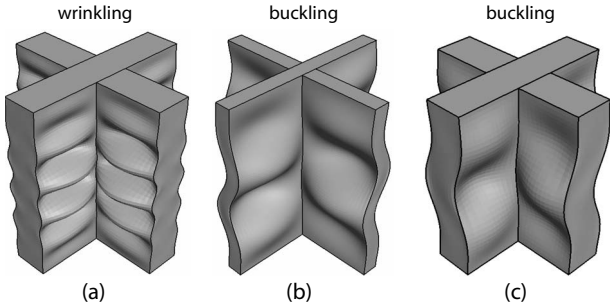

Fig. 6 Finite element predictions of the first eigenmode extracted for the specimen with (*a*) *l*=30 mm and *t*=0.2 mm, (*b*) *l*=75 mm and *t*=0.6 mm, and (*c*) *l*=30 mm and *t*=0.6 mm

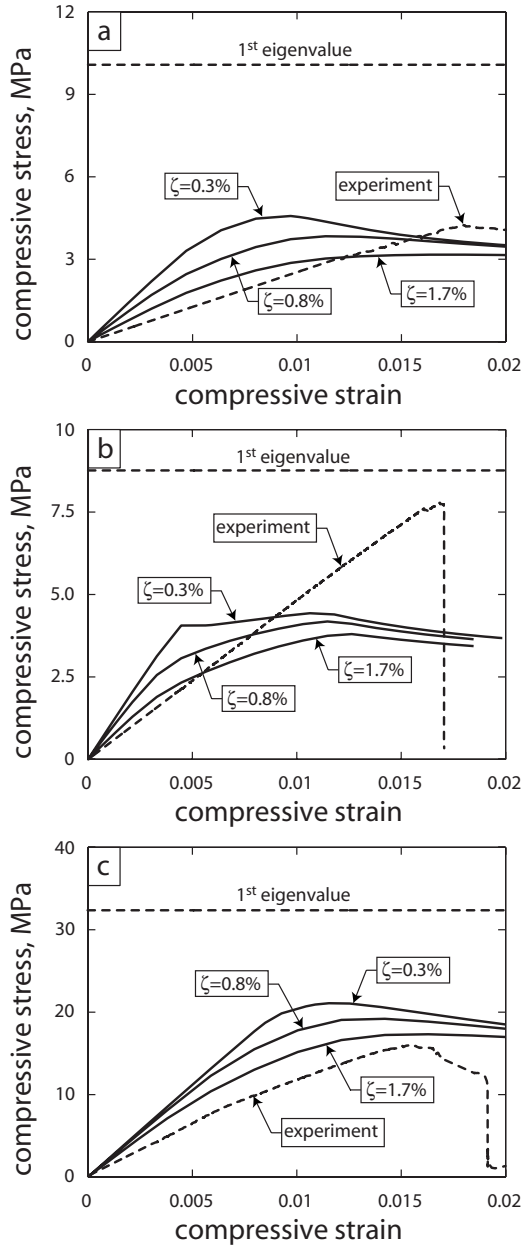

Fig. 7 FE predictions of the compressive response of specimens with (*a*) *l*=30 mm and *t*=0.2 mm, (*b*) *l*=75 mm and *t*=0.6 mm, and (*c*) *l*=30 mm and *t*=0.6 mm. Imperfections in the first eigenmode with maximum amplitude $\varsigma \equiv w/l$ are specified.

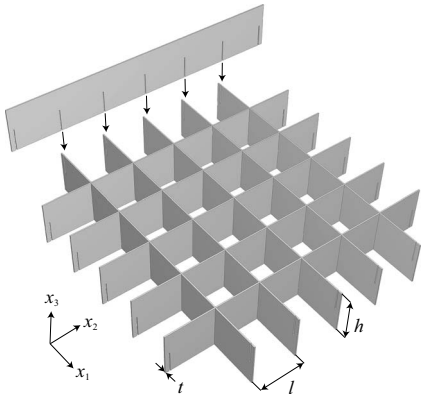

Fig. 8 Sketch of a conventional monolithic square honeycomb showing the geometrical parameters along with the manufacturing technique of the monolithic square honeycomb

defined as follows. The maximum transverse deflection of the walls of the honeycomb is set to $w=\zeta l$, where ζ is in the range of 0–1.7%.

The FE predictions of the compressive stress versus strain responses of the geometries labeled A, B, and C in Fig. 2 are plotted in Fig. 7. (These predictions correspond to the measured responses plotted in Figs. 5(*b*), 5(*d*), and 5(*f*), respectively.) The FE calculations clearly show that the peak stress is sensitive to the magnitude of initial imperfection, and an initial imperfection on the order of $\zeta=0.3\%$ is needed to reproduce the qualitative shape of the measured collapse response.

The finite element predictions of the peak compressive strength of the square honeycombs with $\zeta=0.3\%$ are included in Fig. 5. Mixed agreement is obtained with the measured values. The discrepancy between the measurements and FE predictions is largest for the specimens with $l \geq 60$ mm. For these specimens it would be necessary to consider a smaller imperfection in order to obtain the measured value of peak load. A quantification of the actual imperfections within the macroscopic sandwich panel is difficult to achieve in view of the 3D nature of the structure. This is suggested as a topic of future study using, for example, a computed axial tomography (CAT) scan machine but is not pursued further here.

5 Comparison of the Measured Compressive Strength for Square Honeycombs With Sandwich Walls and With Monolithic Walls

It is instructive to explore the degree to which a hierarchical sandwich construction is advantageous over a more conventional honeycomb. Here, we compare the through-thickness compressive strength of a macroscopic sandwich panel with a square honeycomb core made from monolithic plates with the compressive strength of a macroscopic sandwich panel with a square honeycomb core made from sandwich plates. An additional series of compressive tests has been performed for square honeycombs made from a monolithic, woven glass fiber/epoxy composite. The architecture is identical to that reported above for the foam-cored sandwich plates, but now the square honeycomb is constructed with the foam core absent. It is unclear a priori whether the presence of the foam core elevates or depresses the compressive strength: The presence of a foam core raises the bending stiffness D in Eq. (6) but it lowers the shear stiffness of the section.

Monolithic square honeycombs with 6×6 cells were manufactured from eight harness satin weave E-glass laminate of thickness $t=0.4$ mm using micromilling machining and epoxy bonding, see Fig. 8 for details of the geometric parameters and a sketch of the manufacturing route. The cell aspect ratio of the specimens was maintained at $h/l=1$. The cell size l was varied from 10.4 mm to

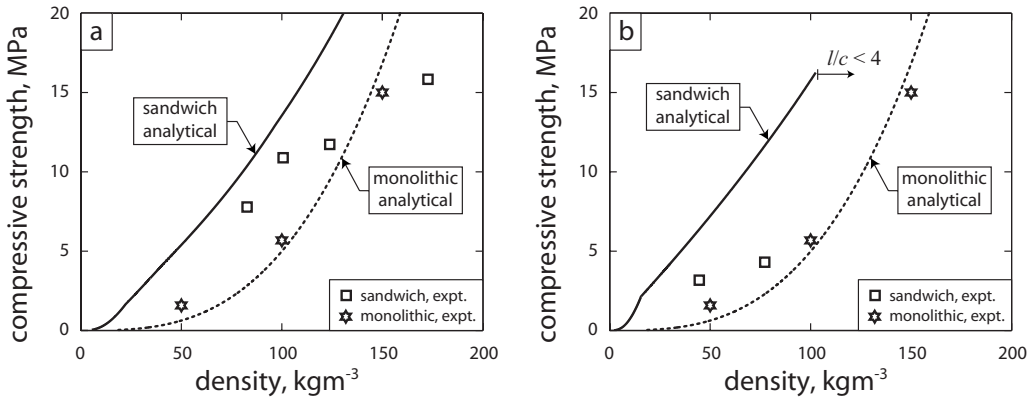

Fig. 9 Comparison between the measured and predicted compressive strength of square honeycombs made from monolithic GFRP laminates and sandwich walls with face sheets of (*a*) $t=0.6$ mm and (*b*) $t=0.2$ mm

31.3 mm in order to obtain three core densities of 50 kg m^{-3}, 100 kg m^{-3}, and 150 kg m^{-3}. Again, aluminum alloy face sheets of thickness 3 mm were bonded to the top and bottom of the square honeycomb using the structural adhesive 3M Scotch-Weld DP490.

Three nominally identical specimens were tested for each core density, and the measured strength varied by only 10% for a given core density. A postmortem visual examination of the failed specimens suggested that each failed by elastic buckling of the honeycomb walls. The average compressive strengths are compared with those of the hierarchical square honeycombs of face thickness $t=0.6$ mm in Fig. 9(*a*). Likewise, the average compressive strengths are compared with those of the hierarchical square honeycombs of face thickness $t=0.2$ mm in Fig. 9(*b*).

The analytical predictions of elastic buckling strength (Eq. (5)) for the monolithic and hierarchical honeycombs have been added to Fig. 9. For the monolithic honeycomb, the analytical model of Ericksen and March [10] is again employed but with

$$D = \frac{\sqrt{E_{1f}E_{3f}}}{1-\nu_{13f}\nu_{31f}}\frac{t^3}{12} \tag{11}$$

This prediction is in good agreement with the measured strengths. As already noted, bifurcation calculation of Ericksen and March [10] is nonconservative for the hierarchical honeycombs.

We note from Fig. 9 that there is a small advantage in using the hierarchical honeycomb over the monolithic honeycomb at sufficiently low core densities. But this comparison is for the case of a foam core of low modulus. As discussed in Sec. 2, additional structural advantages are expected by considering a hierarchical honeycomb for the choice of a stiffer foam core.

6 Concluding Remarks

The hierarchical sandwich panel with a square honeycomb core introduced in this study shows promise as it has a substantially higher through-thickness compressive strength than an equivalent sandwich panel with a monolithic composite core. The compressive strength of the hierarchical sandwich panel is dictated by a set of competing failure modes and these are best illustrated in the form of a collapse map, with geometry as axes. Analytic models are presented here for the competing collapse modes; these have limited accuracy due to the presence of geometric imperfections. Finite element simulations can give improved accuracy but these require as input the level of imperfection. A characterization of the imperfections remains a challenging task.

Acknowledgment

The authors are grateful to the Engineering and Physical Sciences Research Council, UK for financial support.

References

[1] Fairbairn, W., 1849, *An Account of the Construction of the Britannia and Conway Tubular Bridges*,Weale, London, UK.
[2] Allen, H. G., 1969, *Analysis and Design of Structural Sandwich Panels*, Pergamon, Oxford, UK.
[3] Zenkert, D., 1995, *An Introduction to Sandwich Construction*, EMAS, London, UK.
[4] Gibson, L. J., and Ashby, M. F., 1997, *Cellular Solids, Structure and Properties*, 2nd ed., Cambridge University Press, Cambridge, UK.
[5] Deshpande, V. S., Fleck, N. A., and Ashby, M. F., 2001, "Effective Properties of the Octet-Truss Lattice Material," J. Mech. Phys. Solids, **49**, pp. 1747–1769.
[6] Zhang, J., and Ashby, M. F., 1992, "The Out-Of-Plane Properties of Honeycombs," Int. J. Mech. Sci., **34**, pp. 475–489.
[7] Côté, F., Deshpande, V. S., Fleck, N. A., and Evans, A. G., 2004, "The Out-Of-Plane Compressive Behavior of Metallic Honeycombs," Mater. Sci. Eng., A, **380**, pp. 272–280.
[8] Côté, F., Deshpande, V. S., and Fleck, N. A., 2006, "The Shear Response of Metallic Square-Honeycombs," J. Mech. Mater. Struct., **1**, pp. 1281–1299.
[9] Budiansky, B., 1999, "On the Minimum Weights of Compression Structures," Int. J. Solids Struct., **36**, pp. 3677–3708.
[10] Ericksen, W. S., and March, H. W., 1958, "Effects of Shear Deformation in the Core of a Flat Rectangular Sandwich Panel. Compressive Buckling of Sandwich Panels Having Dissimilar Facings of Unequal Thickness," US Forest Product Laboratory, Report No. 1583-B.
[11] Fleck, N. A., 1997, "Compressive Failure of Fiber Composites," Adv. Appl. Mech., **33**, pp. 43–117.
[12] ASTM D3410/D3410M-03, Standard Test Method for Compressive Properties of Polymer Matrix Composite Materials With Unsupported Gage Section by Shear.
[13] Khashaba, U. A., 2004, "In-Plane Shear Properties of Cross-Ply Composite Laminates With Different Off-Axis Angles," Compos. Struct., **65**, pp. 167–177.
[14] McIntyre, M. E., and Woodhouse, J., 1988, "On Measuring the Elastic and Damping Constants of Orthotropic Sheet Materials," Acta Metall., **36**, pp. 1397–1416.
[15] Deshpande, V. S., and Fleck, N. A. J., 2000, "Isotropic Constitutive Models for Metallic Foams," J. Mech. Phys. Solids, **48**, pp. 1253–1283.